2020 American Control Conference
Denver, CO, USA, July 1-3, 2020

Optimal Exploration and Charging for an Autonomous Underwater Vehicle with Energy-Harvesting Kite

James Reed[1], Joshua Daniels[2], Ayaz Siddiqui[3], Mitchell Cobb[4], and Chris Vermillion [5]

Abstract— **This paper examines the control of an autonomous underwater vehicle (AUV) with a deployable energy-harvesting kite for oceanographic observation and surveillance. The proposed design and control strategies specifically address objectives of achieving high-payload, long-endurance AUV operation through the deployment of an energy-harvesting kite while the AUV is anchored to the seabed, followed by the retraction of the kite for continued operation of the AUV. While deployed, the kite executes power-augmenting cross-current flight motions, using a hierarchical controller. When the AUV is in motion and the kite is retracted, a dynamic programming-based controller is used to select charging locations that minimize total charging time when traversing a prescribed mission path. Focusing on oceanographic observation along a Gulf Stream transect, using a hindcast model of the Gulf Stream current resource, the paper demonstrates the efficacy of the proposed control approach, as compared to several non-optimized alternatives.**

I. Introduction

There has been a significant growing interest in long-duration, high-payload autonomous underwater vehicles (AUVs) for oceanographic observation (see [1], [2], and [3]), along with a significant recent push within the defense community for high-endurance, low-observability AUVs for surveillance and anti-submarine warfare (see [4] and [5]). In the aforementioned applications, the AUVs would be tasked with operating undetected for long periods of time to gather tactical oceanographic data, tracking and trailing submarines, and detecting mines [6].

A significant body of literature has looked at the design and control of AUVs and AUV networks for observational, surveillance, and warfare applications. For example, [7] and [8] focus on the use of an AUV for oceanographic observation, collecting measurements such as temperature, current profile, bathymetry, and ocean floor mineral composition. This work thoroughly investigates feasible AUV designs for data acquisition but does not address challenges of mission planning, control, and low observability. Solutions presented by [9] and [10] investigate the use of AUVs of limited endurance to perform surveillance tasks through use of a cooperative robotic network. Drawbacks of this solution include short mission life and high observability during recovery and charging stages.

One option for achieving the goal of long endurance is to design an AUV that can periodically harvest energy from its surrounding environment, without significant disruption to its core mission due to recharging times. In fact, previous work by [1], [2], and [3] has investigated the use of energy-harvesting AUVs that harvest energy when anchored (through on-board rotors that operate as turbines during this regime) and can relocate to accommodate the shifting nature of the flow resource. However, the aforementioned results focus solely on maximizing harvested energy, rather than the mission-oriented control strategy necessary to cover large distances in short amounts of time. Furthermore, this conceptual design requires hundreds of meters of on-board anchor line and ultimately only yields 30 $\frac{W}{m^2}$ of turbine swept area in a 0.5 $\frac{m}{s}$ flow speed.

One candidate mechanism for circumventing the low power per unit area that can be harvested by fixed turbines lies in the use of energy-harvesting kites that execute power-augmenting *cross-current* motion [11] (figure-8 patterns perpendicular to the prevailing flow). As demonstrated mathematically in [11] and experimentally through companies such as Minesto, Ltd. [12] and Windlift, LLC [13], efficient cross-current flight can routinely produce an order of magnitude more power than a stationary system of the same size. These systems can harvest fluid energy from either of two mechanisms:

- *On-board turbines*, where a turbine or turbines are attached to the kite, and energy is transmitted to a base station via a conductive tether;
- *Ground-based generators*, where a motor/generator is attached to a winch, which spools out tether under high tension (which is achieved through high-lift cross-current flight) and spools in tether under low tension (which is achieved through low-lift flight), thereby resulting in a net positive energy output.

In order to achieve persistent operation and minimal recharging time through highly efficient energy harvesting, along with low observability through compact size, this work studies an AUV that can deploy a small energy-harvesting kite for periodic recharging. The conceptual system considered in this work consists of two components: (i) an AUV, depicted in Fig. 1, which consumes energy to move around and explore the environment, and (ii) a deployable kite system, shown in Fig. 1, which harvests energy from

This research was supported by the North Carolina Coastal Studies Institute's Renewable Ocean Energy Program.

[1]James Reed is an undergraduate at North Carolina State University jcreed2@ncsu.edu.

[2]Joshua Daniels is an undergraduate student at North Carolina State University jldanie5@ncsu.edu.

[3]Ayaz Siddiqui is a PhD candidate at North Carolina State University asiddiq2@ncsu.edu.

[4]Mitchell Cobb is a PhD candidate at North Carolina State University mcobb@ncsu.edu.

[5]Chris Vermillion is an Associate Professor in the Department of Mechanical and Aerospace Engineering at North Carolina State University, Raleigh, NC 27695, USA cvermil@ncsu.edu. He is also a technical advisor and equity stakeholder for Altaeros Energies, Inc. and Windlift, LLC

the prevailing flow while the AUV is anchored. Thus, the AUV exhibits hybrid operation consisting of *charging*, where the AUV is moored and the kite is deployed to a favorable location within the water column and executes cross-current flight in order to generate power and charge the batteries, and *exploration*, where the kite is retracted and the AUV moves through the environment.

To fufill the objectives of this work, two important control challenges exist:

- A *high-level* mission planning problem of selecting optimal charging locations that minimize cumulative recharging time;
- A *low-level* flight control problem of guaranteeing robust, high-power cross-current flight across the full spectrum of flow conditions within the mission domain.

In this paper, we address both of these challenges. Specifically, after presenting the basic design parameters and dynamic models for the AUV and kite, we detail a dynamic programming (DP) mission approach that is used to minimize cumulative recharging time. We also introduce a hierarchical cross-current flight controller that is shown to yield robust power-augmenting flight over the spectrum of flow conditions experienced. Using a hindcast oceanographic resource model for the Gulf Stream adjacent to North Carolina provided by [14], we demonstrate the efficacy of the proposed mission planning and control algorithms in realistic flow data. Furthermore, we compare our results against more naive mission planning strategies, as well as non-cross-current energy-harvesting strategies, demonstrating that our control approach requires significantly reduced charging time.

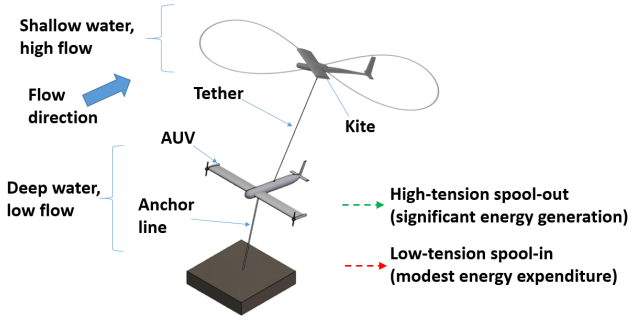

Fig. 1: The AUV will deploy the kite during charging mode. In exploration mode, the kite is retracted and the anchor is reeled in allowing the AUV to perform primary mission objectives.

II. Plant Model

The dynamic model of the AUV used in this work has been developed to capture the essential features of the optimal exploration and charging problem while suppressing many elements of the significant, but complex kite launch-land flight control problem, which while important, lies outside the scope of this work. Key modeling simplifications used to develop this optimization-oriented model are as follows:

1) The AUV moves at a specified velocity while moving between anchor positions.
2) During the charging sequence, the AUV is rigidly anchored to the sea floor.
3) The transition from the charging phase to the exploration phase (and vice versa) is handled by a lower level controller, which requires a fixed amount of time during which zero net energy is generated.

Note that this first assumption implies that the motion of the AUV follows very simple kinematics; position is merely calculated through direct integration of velocity. Furthermore, at any moment we simulate *either* the AUV, or the tension-based, cross current kite (CCK) system, but the two models never operate simultaneously and there is no coupling between their dynamics.

A. Tension-Based, Cross Current Kite Dynamics

The CCK is modeled as a combination of two elements:

- A rigid lifting body wherein forces and moments are calculated from lift, drag, buoyancy, and gravity;
- A lumped mass tether model whose links are characterized as non-compressive spring-damper systems, as in [15] .

The coordinate system used for the kite, $\hat{k}$, specified by the point k at the center of mass (CM) of the kite, and the orthonormal unit vectors $\vec{x}_k$, $\vec{y}_k$, and $\vec{z}_k$ along with the coordinate system of the AUV, with point A at the CM of the AUV and the unit vectors $\vec{x}_{AUV}$, $\vec{y}_{AUV}$, and $\vec{z}_{AUV}$, are shown in Fig. 2. The state variables describing the position and orientation (and their time derivatives) of coordinate system $\hat{k}$ relative to coordinate system $\hat{A}$ evolve according to standard nonlinear equations of motion:

$$\dot{\vec{\mu}} = f(\vec{\mu}, \vec{\omega}) \tag{1}$$

$$\mathrm{J}\dot{\vec{\omega}} = \vec{M}_{Net} - \vec{\omega} \times \mathrm{J}\vec{\omega} \tag{2}$$

$$\dot{\vec{x}} = \mathrm{R}(\vec{\mu})\vec{v} \tag{3}$$

$$\mathrm{M}\dot{\vec{v}} = \left(\vec{F}_{Net}(t) - \vec{\omega} \times \vec{v}\right), \tag{4}$$

where $\vec{\mu} \triangleq [\ \phi \quad \theta \quad \psi]^T$ represents the vector of roll (ϕ), pitch (θ), and yaw (ψ) Euler angles . The matrix $\mathrm{J} \in \mathbb{R}^{3\times3}$ is the inertia matrix, and $\vec{M}_{Net}$ is the sum of all applied moments expressed in the $\hat{k}$ frame. Here, the position vector, $\vec{x} \in \mathbb{R}^3$, is the vector from the point k to the point A, expressed in the $\hat{A}$ frame. The vector $\vec{v}$ is the associated velocity, expressed in the $\hat{k}$ frame. The matrix $\mathrm{R} \in \mathbb{R}^{3\times3}$ is the rotation matrix, calculated based on $\vec{\mu}$, that describes the relative rotation of $\hat{A}$ and $\hat{k}$. The variable $\mathrm{M} \in \mathbb{R}^{3\times3}$ is the diagonal mass matrix, $\vec{F}_{Net}$ is the sum of all forces applied to the kite expressed in the $\hat{k}$ frame, $\vec{\omega} \triangleq [\ \omega_x \quad \omega_y \quad \omega_z]^T$ is the angular velocity of $\hat{k}$ relative to $\hat{A}$. Finally, the function $\vec{f}(\vec{\mu}, \vec{\omega})$ is given by:

$$\vec{f}(\vec{\mu}, \vec{\omega}) = \begin{bmatrix} \omega_x + \omega_y \sin(\phi)\tan(\theta) + \omega_z \cos(\phi)\tan(\theta) \\ \omega_x \cos(\phi) - \omega_z \sin(\phi) \\ \left(\omega_y \sin(\phi) + \omega_z \cos(\phi)\right)\sec(\theta) \end{bmatrix}. \tag{5}$$

The kite is subject to forces and moments resulting from four fluid dynamic surfaces (a port wing, starboard wing, horizontal stabilizer and vertical stabilizer), buoyancy, gravity, and the tether. These forces and moments are calculated

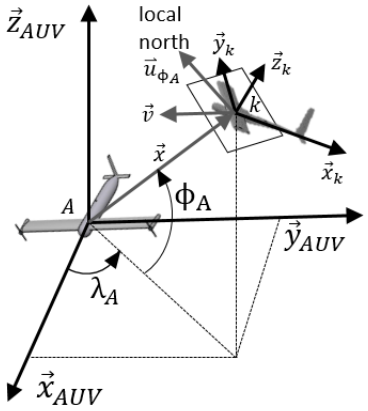

Fig. 2: AUV and kite coordinate systems, $\hat{k}$ and $\hat{A}$, along with spherical coordinate angles λ_A and ϕ_A.

as:

$$\begin{aligned}\vec{F}_{Net} =&\vec{F}_{Thr} + (V\rho - m)\, g\vec{z}_{AUV} \\ &+ \frac{1}{2}\rho A_r \sum_{i=1}^{4} \|\vec{v}_{a_i}\|^2 \left(C_{L,i}\vec{u}_{L,i} + C_{D,i}\vec{u}_{D,i}\right)\end{aligned} \tag{6}$$

$$\vec{M}_{Net} = \frac{1}{2}\rho A_r \sum_{i=1}^{4} \|\vec{v}_{a_i}\|^2 \vec{r}_{a_i} \times \left(C_{L,i}\vec{u}_{L,i} + C_{D,i}\vec{u}_{D,i}\right) \tag{7}$$

where in (6), the first term is the force exerted at the CM by the tether on the kite, the second term describes the net buoyant force, and the last term describes the fluid dynamic forces. Here, V is the volume of the kite, ρ is the fluid density, m is the mass of the system, g is the acceleration due to gravity and A_r is the reference area.

The index, i, refers to each of the four fluid dynamic surfaces. Therefore, the resulting force depends on the apparent flow at the fluid dynamic center of each surface, which is calculated as:

$$\vec{v}_{a_i} = \vec{v}_f(\vec{x} + \vec{r}_{a_i}) - \left(\vec{v} + \vec{\omega} \times \vec{r}_{a_i}\right), \tag{8}$$

where $\vec{v}_f(\cdot)$ is the spatially-varying flow profile, $\vec{v}$ is the velocity of the kite's CM in $\hat{k}$, and $\vec{r}_{a_i}$ is the vector from the CM of the kite to the fluid dynamic center of the i^{th} surface. The fluid dynamic coefficients of equations (6) and (7) are obtained by modeling each fluid dynamic surface independently in the Athena Vortex Lattice (AVL) software [16] and parameterized as functions of the associated control surface deflections, δ_i, as:

$$\begin{aligned}C_{(L,D),i}(\vec{v}_{a_i}) \;=\; & C_{(L_0,D_0),i}(\vec{v}_{a_i}) + C_{(L_1,D_1),i}\delta_i \\ & + C_{(L_2,D_2),i}\delta_i^2\end{aligned} \tag{9}$$

where the control sensitivity coefficients, $C_{L_1,i}$, $C_{L_2,i}$, $C_{D_1,i}$, and $C_{D_2,i}$ are obtained from AVL. The spanwise lift coefficient distributions, $C_{l,i}(y)$, obtained from the software are heuristically corrected to account for nonlinear stall behavior that is not present in AVL. Finally, the variables $\vec{u}_{D,i}$ and $\vec{u}_{L,i}$ represent unit vectors describing the direction of the lift and drag forces at the i^{th} aerodynamic center.

B. AUV Energy Storage System Model

The energy storage system of the AUV is modeled as an on-board battery. The battery's state of charge (SoC) is saturated to lie within a lower limit, E_{min}, and an upper limit, E_{max}. The battery is assumed to expend energy when the AUV is moving, according to a simple work-energy relationship. The battery charges when the AUV is parked, according to the appropriate expression governing the method of energy production (CCK or static flight turbine, SFT). The battery's energy level, E, is calculated according to the following equations:

$$\dot{E}(t) = \begin{cases} -F_d(t)v_{AUV}(t), & v_{AUV}(t) \neq 0, \\ P_{gen}(t), & v_{AUV}(t) = 0, \end{cases} \tag{10}$$

$$E(t) = \int_0^t \begin{cases} 0, & E_{min} \leq E \leq E_{max}, \\ \dot{E}(\tau)d\tau, & \text{otherwise} \end{cases} \tag{11}$$

where $E(t)$ is the energy stored in the battery, $F_d(t)$ is the drag force encountered by the AUV during motion between anchor points, $P_{gen}(t)$ is the instantaneous power generated by the system, and v_{AUV} is speed of the AUV. During the exploration phase, $F_d(t)$ is modeled as

$$F_d(t) = \frac{1}{2}\rho \|\vec{v}_f(\vec{x}_{AUV}) - \vec{v}_{AUV}\|^2 C_d A_{ref}^{AUV}, \tag{12}$$

where ρ is the fluid density, $\vec{v}_{AUV}$ is the velocity vector of the AUV, and A_{ref}^{AUV} is the reference area of the AUV.

In the case of the CCK, instantaneous power produced by the system, $P_{gen}(t)$, is modeled as the product of the net tether force, $||\vec{F}_{thr}||$, and the tether release rate, $U_T(t)$:

$$P_{gen}(t) = ||\vec{F}_{thr}||U_T(t), \tag{13}$$

In the case of the SFT energy generation system, the generated power is calculated as:

$$P_{gen}(t) = \eta_{turb}\frac{N_{turb}}{2}\rho \|\vec{v}_f(\vec{x}_{Turb})\|^3 A_{turb}, \tag{14}$$

where η_{turb} is the turbine efficiency, $\vec{x}_{Turb}$ is the position of the turbine(s), N_{turb} is the number of turbines, and A_{turb} is the reference area of a single turbine.

III. Control Details

The proposed control strategy seeks to achieve rapid exploration of the environment while maintaining the SoC of the on-board battery via efficient kite flight. This can be achieved by (i) strategically selecting recharging locations to lie in areas of favorable flow and (ii) operating the kite robustly and efficiently during deployment. The first goal is achieved by a high-level mission planning controller that uses a DP optimization over a fixed spatial horizon to minimize charging time while satisfying terminal SoC constraints. A lower-level hierarchical flight controller is then used when the kite is deployed to achieve robust, efficient energy-harvesting motions.

A. High Level Controller: Dynamic Programming Based Solution

The high level controller seeks to solve an optimization problem that captures the need to explore the space rapidly while meeting SoC constraints. This is formulated in the following constrained optimization problem, which is applied over a fixed spatial horizon, given an estimate of the flow resource:

$$\underset{\mathbf{u}}{\text{minimize}} \quad J(\mathbf{u}; E(0)) = \sum_{j=0}^{N-1} u(j) + K(u(j)), \tag{15}$$

$$\text{subject to:} \quad E(j+1) = E(i) - E_{loss}(j) + u(j) P_{gen}(j) \tag{16}$$

$$E_{min} \leq E(j) \leq E_{max} \quad \forall\, j \tag{17}$$

$$E(N) \geq E(0) \tag{18}$$

$$u(j) \geq 0 \quad \forall\, j. \tag{19}$$

where j represents a discretized spatial location, $u(j)$ is the charging time at each spatial location, and $\mathbf{u} = [\, u(0) \ldots u(N-1) \,]^T$ is the sequence of charging decisions. The function $K(u(j))$ specifies the time required to deploy the kite ($K(u(j)) = 0$ if $u(j) = 0$ and is $K(u(j)) = K_0$ otherwise), and $E_{loss}(j)$ is the energy expended in moving from spatial location j to $j+1$. The variables $E(j)$ and $P_{gen}(j)$ represent the battery SoC and the generated power, respectively. The first constraint simply characterizes the recharging dynamics, whereas the second constraint imposes saturation limits on the battery SoC. The third constraint requires that the AUV finish the exploration with at least the stored energy it started with, ensuring that the AUV can achieve *persistent* missions. Given the significant distance between subsequent spatial locations, and the substantial available time for computation, we used DP to compute the optimal solution to the mission planning problem.

B. High Level Controller: Baseline Control Strategy

The baseline control strategy used for comparison in this work is implemented as a naive, myopic charging strategy. That is, the system explores until the battery is fully depleted, or does not have enough charge to travel to the next location, and then charges back to the maximum SoC.

C. Low Level Cross Flow Kite Flight Controller

The flight control strategy is ultimately responsible for (i) ensuring that the kite robustly tracks a prescribed figure-8 cross-current flight path, while (ii) spooling in and out in a strategic way that ensures high tension on spool-out and low tension on spool-in.

The figure-8 tracking control strategy contains four levels, as shown in Fig. 3, each of which accept feedback from the plant in calculating their outputs. This modular, hierarchical control structure is based on prior work in [17] and is partitioned into a *path following controller*, a *tangent roll angle controller*, a *desired moment controller* and a *control allocation module*. The spooling mechanics are managed by a winch controller, shown in Fig. 4. This controller employs a state machine to calculate the spooling speed and elevator deflection, the latter of which modulates the angle of attack to generate high tension during spool-out and low tension during spool-in.

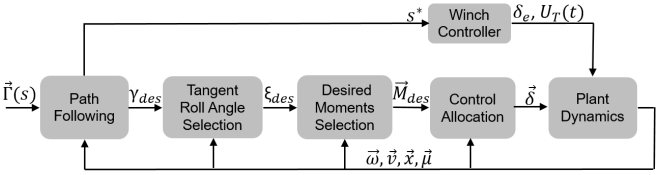

Fig. 3: Four stage hierarchical controller, where $\vec{\delta} = [\delta_a, \delta_r]$.

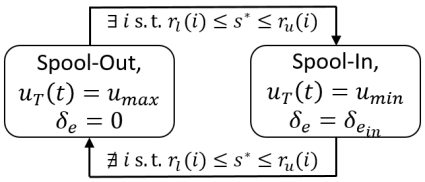

Fig. 4: Winch controller state machine where $r_l \in \mathbb{R}^n, r_u \in \mathbb{R}^n$ are the sets of upper and lower limits on path variable, s, that define the spool-in regions of the path.

1) Path Following Controller: The cross-current path, $\vec{\Gamma}(s)$, is specified in Cartesian coordinates based on the Lemniscate of Booth, which is defined in [17]. The variable s is a path parameter that varies from 0 to 2π describing the figure-8 path. Given this path, this controller calculates a unit vector, $\vec{v}_{des}$, representing the direction of the desired velocity of the system. This desired velocity vector is taken to be a weighted average between the *perpendicular vector*, $\vec{p}^*_\perp$, and the *parallel vector*, $\vec{p}^*_\parallel$. The perpendicular vector is given by

$$\vec{p}^*_\perp = \frac{\hat{p}_\perp}{\|\hat{p}_\perp\|} \quad \text{where} \quad \hat{p}_\perp = \begin{bmatrix} (\vec{\Gamma}(s^*) - \vec{x}) \cdot \vec{u}_{\phi_A}(\vec{x}) \\ (\vec{\Gamma}(s^*) - \vec{x}) \cdot \vec{u}_{\lambda_A}(\vec{x}) \\ 0 \end{bmatrix}. \tag{20}$$

Here, $\vec{u}_{\phi_A}(\vec{x})$ and $\vec{u}_{\lambda_A}(\vec{x})$ are the unit vectors associated with the spherical version of the $\hat{A}$ coordinate system as shown in Fig. 2. Specifically, $\vec{u}_{\phi_A}(\vec{x})$ corresponds to increasing ϕ_A at the current location, and $\vec{u}_{\lambda_A}(\vec{x})$ corresponds to increasing λ_A at the current location. The parallel vector, $\vec{p}^*_\parallel$, is a unit vector that lies parallel to the path at the path variable corresponding to the closest point on the path, s^* and is calculated by

$$\vec{p}^*_\parallel = \frac{\hat{p}_\parallel}{\|\hat{p}_\parallel\|} \quad \text{where} \quad \hat{p}_\parallel = \left.\frac{d\vec{\Gamma}}{ds}\right|_{s=s^*} \tag{21}$$

In equations (20) and (21), the closest point on the path is described by the path variable s^* which minimizes $\alpha(s)$, the angle between the position vector, $\vec{x}$ and the path $\vec{\Gamma}(s)$.

The desired velocity unit vector, $\vec{v}_{des}$ is then calculated as the linearly weighted sum of the perpendicular and parallel vectors according to

$$\begin{aligned} \overline{\alpha}(s^*) &= \min\left\{\alpha(s^*), \alpha_0\right\} \\ \vec{v}_{des} &= \left(1 - \frac{\overline{\alpha}(s^*)}{\alpha_0}\right) \vec{p}^*_\parallel + \frac{\overline{\alpha}(s^*)}{\alpha_0} \vec{p}^*_\perp. \end{aligned} \tag{22}$$

Here, α_0 serves as an upper limit on the possible angle used in the weighting.

The velocity angle, γ which describes the orientation of a given velocity vector on the sphere of radius $\|\vec{x}\|$ at the current position $\vec{x}$, is given by

$$\gamma(\vec{v}) = \text{atan}\left(\frac{\vec{v}\cdot\vec{u}_{\phi_A}(\vec{x})}{\vec{v}\cdot\vec{u}_{\lambda_A}(\vec{x})}\right). \tag{23}$$

The desired velocity angle would then be given by $\gamma(\vec{v}_{des})$.

2) Tangent Roll Angle Selection: The next stage of the flight controller maps $\gamma(\vec{v}_{des})$ to a desired tangent roll angle, ξ_{des}. The tangent roll angle, ξ, which is the angle between $\vec{y}_k$ and the plane tangent to the surface of the sphere of radius $\|\vec{x}\|$ at the kite's position, which will be called the *tangent plane* (shown in Fig. 2) and is calculated as:

$$\tan\left(\xi(\vec{y}_k(t))\right) = \frac{\vec{y}_k\cdot(\vec{u}_{\lambda_A}\times\vec{u}_{\phi_A})}{\sqrt{(\vec{y}_k\cdot\vec{u}_{\phi_A})^2+(\vec{y}_k\cdot\vec{u}_{\lambda_A})^2}}. \tag{24}$$

The desired tangent roll angle is calculated using saturated proportional control, specifically:

$$\xi_{des} = \min\{\max\{k_\gamma\left(\gamma(\vec{v})-\gamma(\vec{v}_{des})\right),\xi_{min}\},\xi_{max}\}, \tag{25}$$

where k_γ is the proportional gain. The adjustment of ξ is responsible for redirecting the kites lift which provides the force necessary to re-align the kite's velocity angle with the target value and ultimately return the kite to its target path.

3) Desired Moment Vector Selection: In selecting the desired moments, we utilize the rolling moment to control tangent roll angle, ξ, and yawing moment to drive aerodynamic side slip angle, β, to a value of zero. Recall that the tether spooling controller articulates the elevator to passively trim the system to a high angle of attack during spool out and a low angle of attack during spool in. Ultimately, the desired moment vector is given by:

$$\vec{M}_{des} = \begin{bmatrix} k_{p_L}e_\xi(t) + k_{i_L}\int_0^t e_\xi(t)d\tau + k_{d_L}\dot{e}_\xi(t) \\ 0 \\ k_{p_N}\beta + k_{i_N}\int_0^t \beta d\tau + k_{d_N}\dot{\beta} \end{bmatrix},$$

where $e_\xi(t) = \xi(\vec{y}_k(t)) - \xi_{des}$, and β is the fluid dynamic side slip angle.

4) Control Allocation Module: In order to map the desired moment vector to the necessary control surface deflections, we invert an approximation of the deflection-moment mapping used in the plant model. This approximation is calculated by neglecting the effect of angular velocity on the apparent flow at each fluid dynamic surface and then linearizing to obtain the following expression:

$$\vec{M}_{net} = \vec{M}_o + [\text{A}]\vec{\delta}, \tag{26}$$

where $\vec{\delta} \triangleq [\ \delta_a\ \delta_e\ \delta_r]^T$ represents the deflection angles of the ailerons, elevator, and rudder, respectively. The variable $\vec{M}_o$ is given by:

$$\vec{M}_o = \frac{1}{2}\rho A_r\|\vec{v}_a\|^2\sum_{i=1}^{4}\vec{r}_{a_i}\times(C_{L_o,i}\vec{u}_{L,i} + C_{D_o,i}\vec{u}_{D,i}) \tag{27}$$

and the matrix [A] is formed by re-arranging the cross products and deflection angles in equations (7) and (9) into a matrix form where the results of the cross products form the columns of the matrix,

$$\begin{aligned} A &= \frac{1}{2}\rho A_r\|\vec{v}_a\|^2\left[\vec{a}_1-\vec{a}_2,\vec{a}_3,\vec{a}_4\right] \quad \text{where} \\ \vec{a}_i &= \vec{r}_{a_i}\times(C_{L_1,i}\vec{u}_{L,i}+C_{D_1,i}\vec{u}_{D,i})\ ,\ i\in\{1,2,3,4\}. \end{aligned} \tag{28}$$

This results in a system of three equations and three unknowns, which is solved at each time step to compute $\vec{\delta}$.

IV. Results

TABLE I: Parameters used in simulation.

Variable	Description	Value	Units
A_{ref}^{AUV}	Reference area of the AUV	11	m^2
A_r	Reference area of the kite	10	m^2
A_{turb}	Turbine swept area	4	m^2
N_{turb}	Number of turbines	2	-
η_{turb}	Turbine efficiency	0.5	-
E_{max}	Maximum allowable battery energy	6.5	kWh
E_{min}	Minimum allowable battery energy	0	kWh
v_{AUV}	Maginitude of AUV velovity	1.25	ms^{-1}
ρ	Fluid density	1000	kgm^{-3}
C_d	AUV drag coefficient	0.085	-
X_{tot}	Total transect length	106	km
X_{incr}	Transect length increment	1.06	km
K_0	Time cost to deploy and retract the kite	600	s

The combined high-level mission planning algorithm and low-level kite control algorithm were simulated based on an oceanographic hindcast model described in [14]. This realistic spatiotemporal data represents a two-dimensional planar slice (transect) of the Gulf Stream off the coast of North Carolina, shown in Fig. 5. Fig. 6 shows the maximum magnitude of the flow speed within the water column as a function of longitudinal position along the transect.

For the simulations studied in this paper, the mission is defined as a complete traversal of the transect, returning to the starting position. Our simulation results examine a DP charging controller with both a CCK and a SFT, as well as a baseline charging controller with both a CCK and SFT for comparison. The parameters used in the four simulations are shown in Table I.

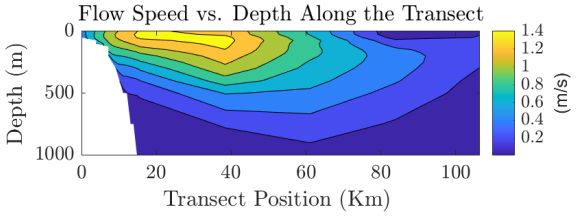

Fig. 5: The flow speed as a function of transect position and depth. This data was collected on October 19^{th}, 2015 at 15:00:00.

A. Simulation Results

The time taken to cross and return across the transect is shown in Fig. 7a and Fig. 7b for both methods of energy

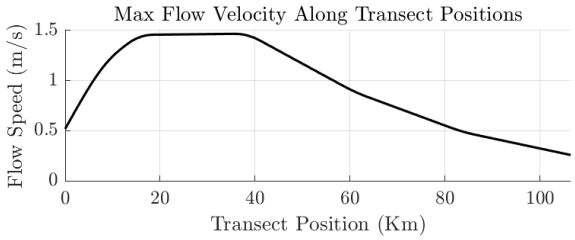

Fig. 6: The above figure depicts the maximum flow speed in the water column at each transect discretization. This data depicts the flow on October 19th, 2015 at 15:00:00.

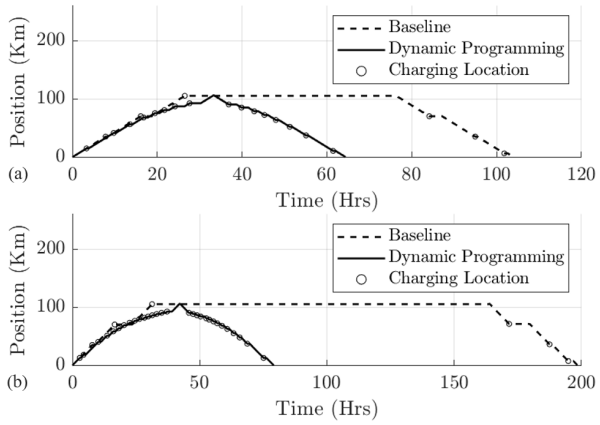

Fig. 7: Time versus position for both the dynamic programming solution and the baseline solution for an AUV with a CCK in (a) and a SFT in (b).

generation. The DP solution charging strategy allowed the AUV to cross and return in 64.4 hours and 79.0 hours for the CCK and SFT methods respectively, while the baseline charging strategy took 104 hours and 198 hours for the CCK and SFT methods respectively. It is clear from these figures the best simulated solution for an AUV repeatedly crossing the Gulf Stream uses a CCK energy generation method and a charging strategy prescribed by the DP solution. Fig. 8a and Fig. 8b show the charging strategy for the AUV using the CCK and SFT method of energy generation respectively from the dynamic programming optimization.

V. Conclusion

In this paper, we investigate the optimal charging strategy and method of energy harvesting for a perpetual endurance AUV. We simulated a dynamical programing based and naive control strategy as applied to both a CCK and SFT. In both instances the DP solution outperformed the baseline charging strategy. Furthermore the CCK enabled faster transect crossings by reducing charging time.

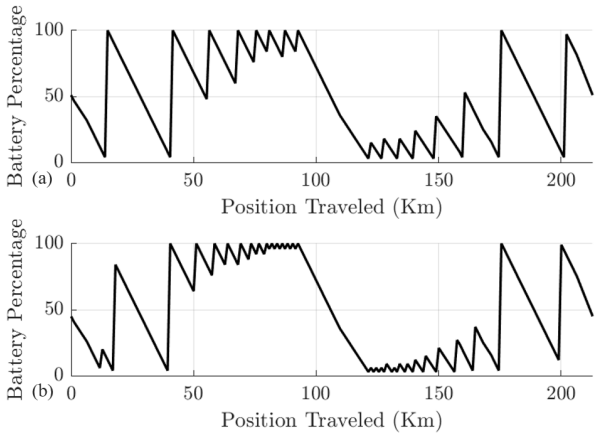

Fig. 8: Percentage of total battery energy versus transect position from the dynamic programming solution for an AUV with a CCK in (a) and a SFT in (b).

References

[1] S. Bin-Karim, M. Muglia, A. Mazzoleni, and C. Vermillion, "Control of a relocatable energy-harvesting autonomous underwater vehicle in a spatiotemporally-varying gulf stream resource," in *2018 Annual American Control Conference (ACC)*, 400 W Wisconsin Ave, Milwaukee, WI, June 2018, pp. 2575–2580.

[2] S. Tandon, S. Divi, M. Muglia, C. Vermillion, and A. Mazzoleni, "Modeling and dynamic analysis of a mobile underwater turbine system for harvesting marine hydrokinetic energy," *Ocean Engineering*, vol. 187, p. 106069, 2019.

[3] S. Bin-Karim, M. Muglia, and C. Vermillion, "Centralized position optimization of multiple agents in spatiotemporally-varying environment: a case study with relocatable energy-harvesting autonomous underwater vehicles in the gulf stream," in *Conference on Control Technology and Applications (CCTA)*, City University of Hong Kong, Hong Kong, 2019.

[4] Defense Advanced Research Projects Agency. [Online]. Available: https://www.darpa.mil/program/manta-ray

[5] B. Fletcher, "New roles for UUVs in intelligence surveillance, and reconnaissance," Space and Naval Warfare Systems Center San Diego CA, Tech. Rep., 2000.

[6] B. Fletcher, "UUV master plan: a vision for navy UUV development," in *OCEANS 2000 MTS/IEEE Conference and Exhibition. Conference Proceedings (Cat. No.00CH37158)*, vol. 1, Sep. 2000, pp. 65–71 vol.1.

[7] M. Dhanak, E. An, K. Holappa, and S. Smith, "Using small AUV for oceanographic measurements," in *Oceans '99. MTS/IEEE. Riding the Crest into the 21st Century. Conference and Exhibition. Conference Proceedings (IEEE Cat. No.99CH37008)*, vol. 3, Sep. 1999, pp. 1410–1417 vol.3.

[8] N. Wakita, K. Hirokawa, T. Ichikawa, and Y. Yamauchi, "Development of autonomous underwater vehicle (AUV) for exploring deep sea marine mineral resources," *Mitsubishi Heavy Industries Technical Review*, vol. 47, no. 3, pp. 73–80, 2010.

[9] G. Ferri, A. Munafò, A. Tesei, P. Braca, F. Meyer, K. Pelekanakis, R. Petroccia, J. Alves, C. Strode, and K. LePage, "Cooperative robotic networks for underwater surveillance: an overview," *IET Radar, Sonar Navigation*, vol. 11, no. 12, pp. 1740–1761, 2017.

[10] W. K. G. Seah, Hwee-Xian Tan, Zheng Liu, and M. H. Ang, "Multiple-UUV approach for enhancing connectivity in underwater ad-hoc sensor networks," in *Proceedings of OCEANS 2005 MTS/IEEE*, Sep. 2005, pp. 2263–2268 Vol. 3.

[11] M. Loyd, "Crosswind kite power," *Journal of Energy*, vol. 4, no. 3, pp. 106–111, 1980.

[12] Minesto. [Online]. Available: https://www.minesto.com

[13] Windlift. [Online]. Available: http://www.windlift.com/

[14] K. Chen and R. He, "Numerical investigation of the middle atlantic bight shelfbreak frontal circulation using a high-resolution ocean hindcast model," *Journal of Physical Oceanography*, vol. 40, no. 5, pp. 949–964, 2010.

[15] C. Vermillion, T. Grunnagle, R. Lim, and I. Kolmanovsky, "Model-based plant design and hierarchical control of a prototype lighter-than-air wind energy system, with experimental flight test results," *IEEE Transactions on Control Systems Technology*, vol. 22, pp. 531–542, 2014.

[16] M. Drela and H. Youngren. (2017) AVL. [Online]. Available: http://web.mit.edu/drela/Public/web/avl/

[17] S. Rapp, R. Schmehl, E. Oland, S. Smidt, T. Haas, and J. Meyers, "A modular control architecture for airborne wind energy systems," in *AIAA Scitech 2019 Forum*, 2019, p. 1419.